Bubble-Size Distribution in Fischer-Tropsch-Derived Waxes in a Bubble Column

Bubble sizes were measured for molten wax-nitrogen systems using photography and dynamic gas disengagement. The effects of operating conditions, system geometry and wax type were studied in 0.05- and 0.23-m-diameter by 3-m-tall bubble columns. Both techniques were used with FT-300 wax, while only the dynamic gas disengagement technique could be used with reactor waxes due to their dark color. For FT-300 wax, Sauter mean diameters obtained from photographs taken near the column wall were significantly lower than those obtained from photographs taken near the center. The d_s values obtained from dynamic gas disengagement and photographic (near the column center) methods, for this noncoalescing medium, were in the range 0.5-1.6 mm in the large-diameter column. For reactor waxes, d_s values were significantly higher (1-2 mm for Sasol and 1-5.5 mm for Mobil's reactor wax) and are in agreement with results reported in earlier studies with similar waxes (d_s = 2-4 mm), where different experimental techniques (light transmission or hot wire anemometry) were employed.

Snehal A. Patel
James G. Daly
Dragomir B. Bukur
Kinetics, Catalysis and Reaction Engineering Laboratory
Department of Chemical Engineering
Texas A&M University
College Station, TX 77843

Introduction

The advantages of using a slurry column for Fischer-Tropsch synthesis have been elaborated by several researchers in recent years (e.g., Deckwer et al., 1980; Kölbel, and Ralek, 1980; Satterfield and Huff, 1980; Bukur et al., 1987a). In the slurry bed process, very small catalyst particles are suspended in a molten wax, and a mixture of H_2 and CO (synthesis gas) is passed through in the form of gas bubbles. Bukur et al. (1987a, b) have summarized the findings of studies related to the hydrodynamics of Fischer-Tropsch synthesis in a bubble column reactor. The overall mass transfer rate per unit volume of the dispersion in a bubble column is determined by the liquid-side mass transfer coefficient (k_la), assuming that the gas-side resistance is negligible. In a bubble column, the variation in k_la primarily results from variations in the interfacial area (Fan, 1989). The specific gas-liquid interfacial area is related to the average gas holdup and the Sauter mean bubble diameter, d_s, by

$$a = \frac{6\epsilon_g}{d_s} \tag{1}$$

Extensive work on bubble-size measurements in two-phase systems has been reported in literature and has been reviewed by several authors (e.g., Buchholz and Schügerl, 1979; Shah et al., 1982; Saxena et al., 1988); however, the majority of these studies pertain to the air-water system. Investigations on bubble-size measurements with molten wax as a liquid medium are rather limited (e.g., Calderbank et al., 1963; Quicker and Deckwer, 1981; O'Dowd et al., 1986), and there is some disagreement between bubble-size data reported in these studies. Previous work with this medium has dealt mainly with overall gas holdup and its dependence on operating conditions and system parameters (e.g., Deckwer et al., 1980; Kuo et al., 1985; Sanders et al., 1986; Bukur et al., 1985, 1987a, b; Bukur and Daly, 1987). The general consensus is that some molten wax systems depict an unique behavior: that is, an abundance of very small bubbles are present and high gas holdups are obtained in comparison to other hydrocarbons having similar physical properties. The resulting specific interfacial areas could be an order of magnitude greater than those for the other hydrocarbons (Quicker and Deckwer, 1981). The findings from bubble-size measurement studies with molten waxes are summarized below.

Calderbank et al. (1963) used a light-transmission technique

Correspondence concerning this paper should be addressed to D. B. Bukur.

to measure interfacial areas for Krupp wax at 265°C for gas velocities less than 0.06 m/s in a 0.05-m-diameter column equipped with a ball and cone type sparger. When these data, along with the average gas holdup values reported by them, are used in Eq. 1, Sauter mean bubble diameters in the range of 2–3 mm are obtained. Zaidi et al. (1979) and Deckwer et al. (1980) reported a much lower d_s value, 0.7 mm, for paraffin wax using photography in 0.041- and 0.1-m-diameter columns equipped with 75-μm porous plate spargers (250–270°C, $u_g \leq 0.03$ m/s). Quicker and Deckwer (1981) measured d_s values for FT-300 wax in a 0.095-m-diameter column equipped with a 0.9-mm nozzle. Sauter mean bubble diameters, determined by the photographic method, at 170°C ranged between 1.3 mm (at 0.01 m/s) and 0.6 mm (at 0.035 m/s). More recently, O'Dowd et al. (1986) obtained d_s values for a P-22 wax, and for reactor wax from run 7 in Mobil's pilot-plant slurry reactor (Unit CT-256) using the hot wire anemometer at 250°C and 1.48 MPa. Their d_s values, from a 0.022-m-ID column equipped with a 1-mm orifice plate, for the two waxes were in the range of 2.7 to 3.9 mm for $u_g \leq 0.02$ m/s and are comparable to values reported by Calderbank et al. (1963).

The lower d_s values from the studies conducted by Zaidi et al., Deckwer et al., and Quicker and Deckwer, cannot be attributed to the limitation of the photographic technique, i.e., its bias towards small bubbles (in the vicinity of the wall). This is because all of these studies were conducted in the homogeneous bubbly regime (Quicker and Deckwer, 1981), where the dispersion is expected to be radially uniform. A possible cause for the differences could be the behavior of the medium itself. Bukur et al. (1987b) have shown that, despite similar physical properties, different waxes have dissimilar hydrodynamic behavior. This was attributed to differences in the coalescence-promoting properties of the various waxes.

The objective of this study was to investigate the effect of operating conditions, system geometry, and wax type on bubble-size distributions. The measurements were made using two different techniques, photography and dynamic gas disengagement (DGD). We investigated the effect of radial position on d_s by taking photographs of the dispersion near the column wall as well as near the center of the column through a special viewing port. The effect of wax type was studied using FT-300 wax (a noncoalescing medium), and reactor waxes (i.e., high-molecular-weight hydrocarbons produced during the synthesis).

Experimental Equipment and Methods

Apparatus

Two glass bubble columns (0.05-m-ID and 0.23-m-ID, 3-m-tall) and a stainless steel column (0.24-m-ID by 3-m-tall) were used in this study. Similar setups were used with each column, and a detailed description of the apparatus was given elsewhere (Buker et al., 1987a, b). The 0.24-m-ID stainless steel column was equipped with a viewing port located at a height of 1.4 m above the distributor. The port was indented into the column to a depth of 0.03 m from the center of the column. A 40-μm sintered metal plate (SMP), and 2- and 4-mm-orifice plate distributors were used in the 0.05-m-ID column, whereas a 19×2 mm perforated plate distributor was used in the large columns. Majority of the experiments were conducted at 265°C and atmospheric pressure, and a few were made at 200°C to study the effect of temperature. Gas velocities in the range 0.01 to 0.15 m/s were employed in this study. This range includes the homogeneous bubbly flow regime (low gas velocities), and the slug flow regime (0.05 m ID column) or the churn turbulent regime (0.23 m ID column) at higher gas velocities.

The average gas holdup for experiments in the glass columns was calculated using visual observations of the expanded (including any foam present) and static liquid heights. In the stainless steel column, differential pressure measurements from pressure transducers located along the column height were used to estimate the average gas holdup. For a given set of operating conditions, holdup was measured three times. For gas velocities less than 0.05 m/s readings were taken every 30 minutes, whereas for higher gas velocities readings were taken every 20 minutes to ensure that steady-state conditions were achieved. Foam level at the top of the dispersion tends to rise with time. Also, sufficient time must be allowed for small bubbles to propagate into the bulk of the dispersion; otherwise, erroneous holdup and Sauter mean bubble diameter values would be obtained. Photographic and/or dynamic gas disengagement measurements were taken following the last set of readings at a given gas velocity.

Photographic technique

A Canon, AE1/P (SLR) camera was used with Canon auto bellows and a 135-mm Canon lens with a polaroid filter to take photographs. The camera was also equipped with a Vivitar Model 283 flash unit. The optimal arrangement for the 0.05-m-ID column consisted of two 1,000-W Colortran lights placed at angles of 90° with respect to the front of the column in a staggered position (i.e., one 0.15 m above the field of view and the other 0.15 m below the field of view). A shield (flat black metal plate) was placed between the lower light and the field of view. Milar paper was placed between the field of view and the light at the top in order to reduce the glare. Photographs were taken at all gas velocities (0.01 to 0.12 m/s) at heights of 0.5, 1.2 and 2.0 m above the distributor, except when foam filled the entire column (photographs were taken only at 1.2 m for such cases). The flash was used for photographs in the large columns. It was mounted at a distance of 0.25 m from the column at an angle of 45° with respect to the front face of the column. At low gas velocities ($\leq$0.05 m/s) the Canon 135-mm lens mounted on the auto bellows with an extension of 110 mm was employed, whereas at higher velocities (>0.05 m/s) a 50-mm lens with an extension of 70 mm was used. An f/stop of 16 was found to produce the best results. Photographs were taken for all gas velocities at heights of 0.4, 1.1 and 2.0 m above the distributor in the glass column and through the viewing port in the stainless steel column.

A minimum of four photographs were taken at each condition and location, using Kodak's 400 ASA Tri-X Pan film. The area of the column photographed was kept at a minimum (15 × 20 mm) in order to reduce distortions due to the curvature of the column wall. A reference mark, attached to the column wall and in the field of view of the camera, was used for image scaling purposes. Selected photographs were enlarged to 8" × 10" and analyzed on a Zeiss image analyzer equipped with a digitizer and a light pen. The analyzer allowed interactive editing of the image, which made it possible to separate overlapping bubbles. The area equivalent diameter was estimated for each bubble, and the bubble size distribution was obtained. Each distribution

consisted of 60 to 65 bubble classes or groups based on the area equivalent diameter.

The Sauter mean diameter, which is the volume to surface area ratio of the bubbles in the distribution, assuming spherical bubbles, is estimated using

$$d_s = \frac{\sum_{i=1}^{N} n_i d_{bi}^3}{\sum_{i=1}^{N} n_i d_{bi}^2} \tag{2}$$

Dynamic gas disengagement technique

A videocamera and a VCR unit were used to record the drop in liquid level during the disengagement process. A vertical ruler mounted next to the column (in the camera's field of view) was used to obtain the actual heights. After the completion of a run at a given gas velocity, the gas flow was shut off using a solenoid valve and the drop in liquid level recorded. Detailed description of the procedure was given elsewhere (Patel et al., 1989).

The technique has been used by several researchers to determine the gas holdup structure and bubble rise velocities in bubble columns, and was subsequently extended to also include the estimation of Sauter mean diameters (Kuo, 1985; Patel et al., 1989). We have used the technique to determine Sauter mean bubble diameters in several systems including pure *n*-butanol, and aqueous solutions of *n*-butanol or *n*-butanol and carboxymethyl cellulose (Bukur and Patel, 1989), and the air-water system (Patel et al., 1989). The DGD technique, first proposed by Sriram and Mann (1977), assumes that the dispersion is axially homogeneous at the instant when gas flow is interrupted and that there are no bubble-bubble interactions. Patel et al., (1989) have presented a detailed discussion on the theory for this technique, based on two limiting cases:

1. A constant rate process, where the different bubble classes disengage independent of one another.
2. An interactive process, where disengagement of large bubbles retards the disengagement of smaller bubbles.

In the present work, analysis is based on the constant rate process. Only the relevant equations, for analysis of data obtained from DGD measurements, are given here.

The experimentally measured disengagement profile is plotted as normalized height (H/H_o) vs. time, and approximated by a series of straight line segments (2 – 3). Each line segment represents a different bubble size class. The slopes (s_i) and intercepts (b_i) for the different line segments are estimated using linear regression and used in the relationships given below. The first line segment ($i = 1$) represents the disengagement of all of the largest bubbles and some of the smaller bubbles from the remaining classes, whereas the last line segment ($i = N$) represents the disengagement of the smallest bubbles.

The holdup attributed to bubbles in a given class is estimated using

$$\epsilon_{goi} = \frac{H_s}{H_o}\left[\frac{1}{b_{i+1}} - \frac{1}{b_i}\right]; \qquad i = 1 \text{ to N} \tag{3}$$

and the rise velocity of bubbles in a given class is estimated using

$$u_{bi} = \frac{H_o[b_i s_{i+1} - b_{i+1} s_i}{b_i - b_{i+1}}; \qquad i = 1 \text{ to } N \tag{4}$$

The volume fraction of bubbles in a given class is estimated by normalizing the holdup attributed to that class of bubbles, i.e.,

$$f_i = \frac{\epsilon_{goi}}{\epsilon_{go}} \qquad i = 1 \text{ to } N \tag{5}$$

Bubble sizes are estimated from the knowledge of the terminal rise velocity by using appropriate correlations. The correlations used to determine bubble sizes in the present study are summarized in Table 1. For the range of rise velocities not covered by these correlations, bubble diameters were obtained by interpolation. Figure 1 shows the curve used to determine bubble sizes for FT-300 wax at 265°C, with the broken line indicating the interpolated region. For the systems investigated in this work, less than 5% of the rise velocities were in this intermediate region. The correlation by Abou-el-Hassan (1983) was used to estimate small bubble diameter for FT-300 wax, whereas the Peebles and Garber's correlation (1953) was used for reactor

Table 1. Correlations for Estimating Bubble-Size from Bubble Rise Velocity

Reference	Correlation	Range of Applicability
Peebles and Garber (1953)	$d_{bS} = 4.76\left[\frac{\mu_\ell}{\rho_\ell}\right]^{0.41} \frac{u_{b\infty}^{0.78}}{g^{0.59}}$	$2 \le Re \le 4.02\left[\frac{g\mu_\ell^4}{\rho_\ell \sigma_\ell^3}\right]^{-0.214}$
Clift et al. (1978)	$u_b = \left[\frac{2.14\sigma_\ell}{\rho_\ell d_b} + 0.505 g d_b\right]^{0.5}$	$d_b > 1.3\ mm$
Abou-el-Hassan (1983)	$V = 0.75[log\,(F)]^2$	$710 \le \rho_\ell \le 1{,}180\ kg/m^3$ $0.233 \le \mu_\ell \le 59\ mPa\cdot s$
	V = velocity number $= \frac{u_b d_b^{2/3} \rho_\ell^{2/3}}{\mu_\ell^{1/3} \sigma_\ell^{1/3}}$	$0.015 \le \sigma_\ell \le 0.072\ N/m$ $0.1 \le V \le 40$
	F = *flow number* $= \frac{g d_b^{8/3} (\rho_\ell - \rho_g) \rho_\ell^{2/3}}{\mu_\ell^{4/3} \sigma_\ell^{1/3}}$	$1 \le F \le 10^6$

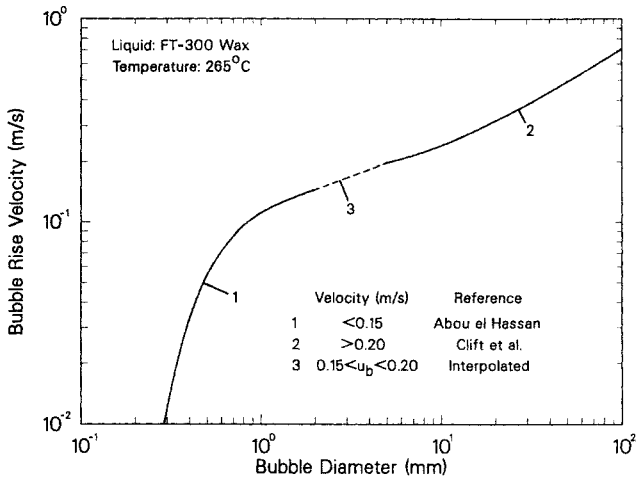

Figure 1. Bubble rise velocity vs. bubble diameter correlation for FT-300 wax.

waxes. The ranges of applicability for these correlations (Table 1) were satisfied in all cases, except for wax density at 265°C. At this temperature, densities of the three waxes were in the range 655 to 681 kg/m^3, and these were slightly below the range of applicability of the Abou-el-Hassan correlation. Finally, the Sauter mean bubble diameter is estimated from

$$d_s = \frac{\epsilon_{go}}{\sum_{i=1}^{N} \epsilon_{goi}/d_{bi}} \tag{6}$$

Materials used

The liquids used in this study were FT-300 wax (average molecular weight of 730) from Dura Commodities Co., New York, reactor wax from Sasol's Arge fixed-bed reactor, and the composite reactor wax from runs 9, 11 and 12 in Mobil's pilot-plant slurry reactor (Unit CT-256). Physical properties for these waxes are summarized in Table 2. Surface tension values for the three waxes have not been reported; however, for a variety of similar waxes, the surface tension values are between 0.021 and 0.027 N/m (Bukur et al., 1987b). We have used a constant value of 0.024 N/m in the present work.

Experimental Results and Discussion

Bubble-size measurements using photography

Molten FT-300 wax is clear and has a water-like appearance in the absence of foam, making it possible to use the photographic technique to measure bubble-size distributions. Photographs were taken at several axial locations in both the 0.05- and 0.23-m-ID glass columns. In the 0.24-m-ID stainless steel column, photographs were taken through the specially constructed window, which was located at a height of 1.4 m above the distributor. Results from these measurements are discussed here in terms of the various effects investigated.

Table 2. Physical Properties of Waxes

Wax Type	Temp. (°C)	Density (kg/m^3)	Viscosity ($mPa \cdot s$)
FT-300 Wax	200	722	4.2
	265	681	2.7
Sasol Wax	200	701	2.9
	265	655	2.0
Mobil Wax	200	716	3.8
	265	674	2.3

Effect of Distributor Type. Figure 2 compares cumulative bubble-size distribution curves obtained with the 2-mm-orifice plate distributor and the 40-μm sintered metal plate (SMP) distributor in the 0.05-m-ID column. The measurements were made at a superficial gas velocity of 0.07 m/s and at a height of 1.2 m above the distributor. These results show that the SMP distributor produced smaller bubbles than did the orifice plate distributor. Comparisons at lower gas velocities are difficult because of the excessive foam produced with the SMP distributor.

Bhavaraju et al. (1978) have defined three regimes of bubble formation at the distributor, based on the gas flow rate (or the orifice Reynolds number, Re_o). For the range of gas velocities used in our study with the 2-mm-orifice plate distributor, Re_o is in the range of 3,350–40,200, and the jet or turbulent regime is applicable for this range of Reynolds numbers. Heijnen and van't Riet (1984) have stated that in this regime the Sauter mean bubble diameter at the orifice (d_s^*) is weakly dependent on the gas flow rate and its value is between 4 and 6 mm. Furthermore, they stated that d_s^* is not influenced by the coalescing or noncoalescing properties of the medium. Studies conducted by Miyahara et al. (1983) show that at high gas flow rates the size of bubbles in the vicinity of the distributor is independent of the orifice diameter, gas flow rate and the physical properties of the medium.

Studies with porous plates (Heijnen and van't Riet, 1984) indicate that d_s^* values for bubbles formed at the distributor in noncoalescing media with these plates are in the order of 0.5–1.0 mm. These studies also show that the size of these bubbles is invariant with gas flow rate.

As the above studies indicate, bubbles produced at the distributor are significantly smaller for the SMP distributor than those produced with the orifice plate distributor. In a noncoalescing medium, where bubble size is dictated predominantly by break-

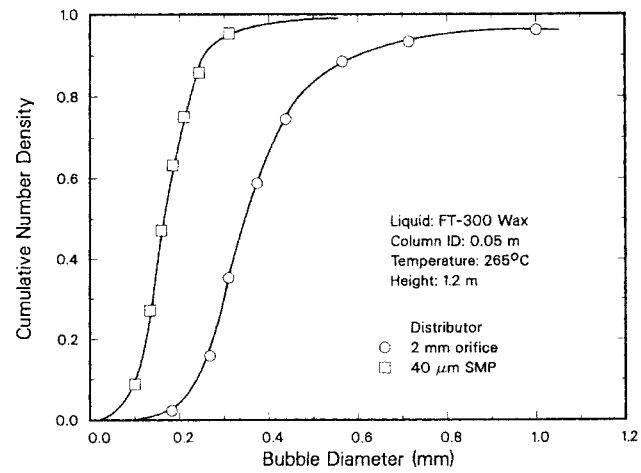

Figure 2. Effect of distributor-type on bubble-size distribution determined by photographic method (at the column wall).

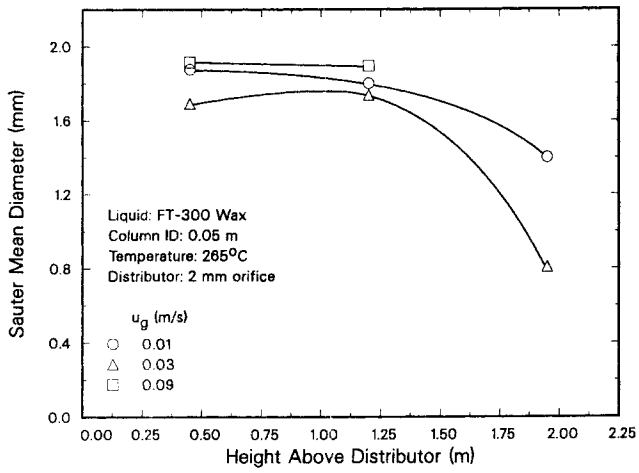

Figure 3. Effect of superficial gas velocity and height above distributor on Sauter mean bubble diameter determined by photographic method (at the column wall).

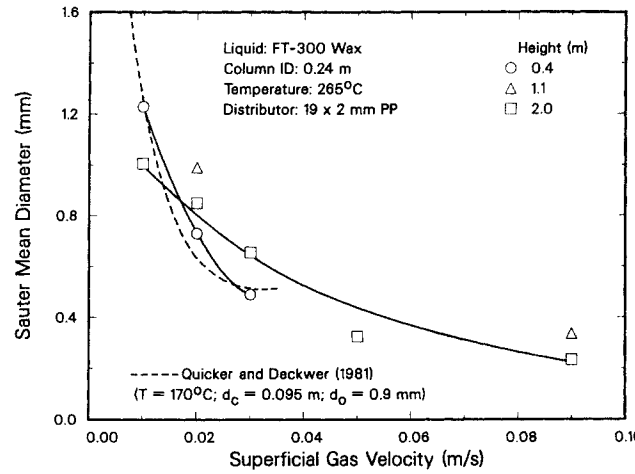

Figure 4. Effect of superficial gas velocity on Sauter mean bubble diameter determined by photographic method (at the column wall).

age, it intuitively follows that the bubble-size distribution at locations further away from the distributor would also show the effect of distributor type. Therefore, the smaller bubbles and the narrower bubble-size distribution observed with the SMP distributor, compared to the distribution with the 2-mm-orifice plate (Figure 2), is in agreement with literature findings. When photographs of the foam were analyzed, it was found that d_s for foam was consistently around 0.5 mm. The bubble-size distribution for foam is relatively narrow and reveals no effect of the type of distributor used.

Effect of Axial Location and Superficial Gas Velocity. Figure 3 shows results from photographs taken in the 0.05-m-ID column equipped with the 2-mm-orifice plate distributor. Results are shown for three different superficial gas velocities, 0.01, 0.03 and 0.09 m/s. Approximately 400–500 bubbles were catalogued and sized at each condition. These results indicate that d_s does not vary significantly in the lower half of the column (up to about 1.2 m above the distributor); however, d_s decreases above this point. The maximum drop in d_s is at a gas velocity of 0.03 m/s, from 1.7 mm at a height of 1.2 m to 0.8 mm at a height of 1.9 m above the distributor. This velocity also coincides with the condition where the greatest amount of foam is produced at the top of the dispersion, and a sharp drop in d_s near the top of the dispersion would be expected.

Effect of superficial gas velocity and axial position on d_s for experiments conducted in the 0.23-m-ID glass column equipped with the 19×2 mm perforated plate distributor is illustrated in Figure 4. Approximately 1,500–1,700 bubbles were catalogued and sized at each condition. These results indicate that the Sauter mean diameter decreases initially as gas velocity is increased and then approaches a constant value at higher gas velocities. At 0.4 m above the distributor, d_s decreases from approximately 1.2 mm at 0.01 m/s to 0.5 mm at 0.03 m/s. At heights of 1.1 and 2.0 m above the distributor, d_s approaches 0.3 mm at a gas velocity of 0.09 m/s. Visual observations of the dispersion support these findings. The sharp drop in d_s as u_g increases from 0.01 to 0.03 m/s is due to the increased amount of foam present at u_g = 0.03 m/s. Results from the work by Quicker and Deckwer (1981) with FT-300 wax in a 0.095-m-ID column are also shown in Figure 4. They took photographs of bubbles along the column wall for experiments performed in the homogeneous flow regime. Their results show that d_s is around 1.5 mm at low gas velocities (0.005 m/s) and it decreases to about 0.5 mm at a gas velocity of 0.035 m/s. d_s values from the current study at a height of 0.4 m above the distributor are in good agreement with the results of Quicker and Deckwer. Also, Zaidi et al. (1979) and Deckwer et al. (1980) have reported d_s values of about 0.7 mm for molten paraffin wax in bubble columns equipped with porous-plate spargers.

Bubble-size distributions obtained from photographs taken near the column wall are not representative of the distribution averaged across the column cross-section. Liquid circulation patterns in the bubble column consolidate the small bubbles near the column wall, whereas the larger bubbles remain in the central core of the dispersion. Experiments conducted by Ueyama et al. (1980) confirm this limitation of the photographic technique. To offset the bias of the technique towards small bubbles, photographs were also taken through a specially constructed window in the 0.24-m-ID stainless steel column. The window is offset into the column to make it possible to photograph the dispersion near the center of the column (approximately 0.03 m from the center of the column). Special care was taken, while designing the window, to minimize the disturbance caused to the flow field in the column. A skirt, directly below the window, formed a hollow cavity that trapped bubbles that were in the dispersion between the wall and the skirt, while allowing bubbles outside this region to rise freely. The trapped gas was released once the cavity was full. The dispersion was photographed during the interval between successive releases of the trapped gas.

Figure 5 shows results from photographs taken through this window. Approximately 1,500–1,700 bubbles were catalogued and sized from two photos at each velocity. The vertical bars in Figure 5 join Sauter mean diameters from the individual photographs, and the solid circles represent d_s values obtained when results from the two photographs were combined. These results represent the bubble-size distribution in the dispersion near the center of the column (as opposed to distributions of the dispersion near the wall of the column, when photographs from the

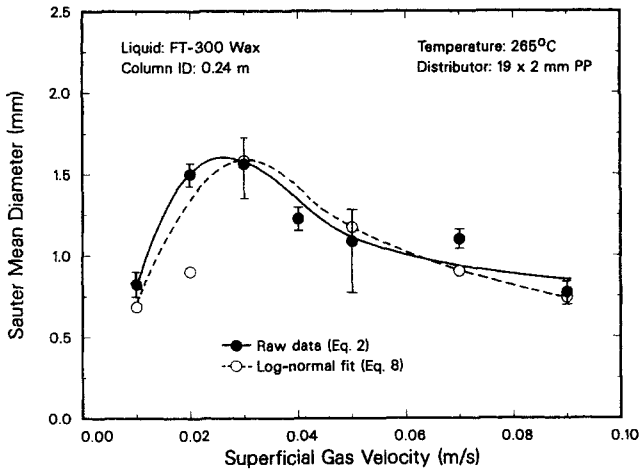

Figure 5. Effect of superficial gas velocity on Sauter mean bubble diameter (at the column center).
Vertical bars join Sauter mean diameters from individual photographs, while solid circles represent Sauter mean diameters when results from the two photos were combined.

glass columns were analyzed). The Sauter mean diameter reaches a maximum value of 1.5 mm at a gas velocity of 0.03 m/s and then stabilizes at 0.8 mm for higher gas velocities (up to 0.12 m/s). Sauter mean diameters from individual photographs compare satisfactorily considering the limitations of this procedure. At low gas velocities (0.01–0.03 m/s), there is some coalescence, which causes the bubble size to increase. However, as gas velocity is further increased, the transition to the churn-turbulent regime takes place and is accompanied by intense mixing, resulting in relatively small bubble sizes.

Akita and Yoshida (1974) and Smith et al. (1983) have shown that the log-normal distribution function adequately represents cumulative bubble-size distributions. The log-normal distribution is given by

$$f(d_b) = \frac{1}{\sigma d_b \sqrt{2\pi}} \exp\left[-\frac{1}{2}\left(\frac{\ln(d_b) - \mu}{\sigma}\right)^2\right] \qquad (7)$$

The Sauter mean bubble diameter for such a distribution can be estimated from the ratio of the third and second moments of such a distribution, which follows from the definition of d_s (Eq. 2). The final expression for d_s is

$$d_s = \exp\left(\mu + \frac{5}{2}\sigma^2\right) \qquad (8)$$

The mean (μ) and standard deviation (σ) of the distribution are estimated from a plot of ln (d_b) vs. cumulative density on probability paper (which should be a straight line). The standard deviation is obtained by taking the inverse of the slope of the straight line, and the mean is obtained by first locating the bubble size corresponding to a cumulative density of 0.5, and then taking the natural log of this value. These estimates for μ and σ can then be used in Eq. 8 to determine d_s.

When bubble-size distributions obtained from photographs taken at the viewing port in the 0.24-m-ID column (combined results from two photographs at each condition) were plotted on probability paper [i.e., ln (d_b) vs. cumulative density], straight lines were obtained for all cases. The mean and standard deviations for each of these distributions were estimated, and d_s values were determined using Eq. 8. These results are in good agreement with d_s values obtained from the original data, using Eq. 2, as shown in Figure 5.

In general, d_s values from measurements made in the 0.05-m-ID column (e.g., Figure 3) are greater than those obtained in the 0.23-m-ID column (e.g., Figure 4). We believe, this is caused, to some extent, by the differences in techniques used in the two columns, rather than by the differences in column diameter alone. It is expected that the fewer bubbles sized from photographs in the smaller-diameter column (1 photograph per condition, 400–500 bubbles), compared to the number of bubbles sized in the larger diameter column (two photographs per condition, 1,500–1,700 bubbles), caused a disproportionate number of larger bubbles to be included in the bubble-size distributions for the small column. This would result in a larger d_s value for the 0.05-m-ID column.

Effect of Radial Position. Results obtained from photographs taken in the 0.23-m-ID glass column (near the column wall) are compared to those obtained from photographs taken in the 0.24-m-ID stainless steel column (near the center of the column) in Figure 6.

Sauter mean diameters from the stainless steel column, taken at a height of 1.4 m above the distributor, are compared with values obtained in the glass column at a height of 2.0 m above the distributor. Values obtained at a height of 2.0 m were used because only limited data were available at a height of 1.1 m in the glass column. Furthermore, d_s values at the two heights for a given gas velocity are similar (Figure 4). In Figure 6, the variation of d_s with normalized radial position, for different gas velocities, is shown. These results indicate that d_s is significantly affected by radial position at all gas velocities, except at 0.01 m/s. At 0.01 m/s, the Sauter mean diameter is approximately the same at the two locations, indicating that the homogeneous bubbly flow prevails under these conditions. At higher gas velocities (>0.01 m/s), circulation patterns begin to develop, and the large bubbles rise in the center of the column, while the small bubbles are entrained in the liquid moving down along the column wall. Ueyama et al. (1980) and Smith et al. (1984) have

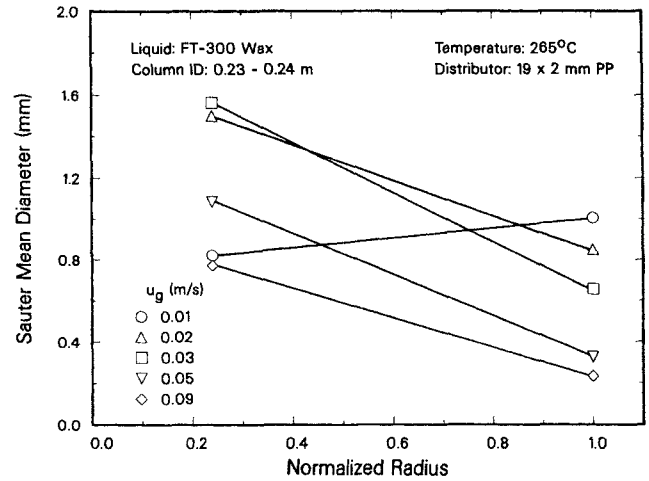

Figure 6. Effect of radial position on Sauter mean bubble diameter determined by photographic method.

found similar gradients in bubble size for the air-water and the aqueous ethanol-nitrogen systems, respectively.

Bubble-size measurements using dynamic gas disengagement

The dynamic gas disengagement technique was used to estimate bubble sizes and the holdup structure of the dispersion with FT-300 wax and reactor waxes. The photographic technique could not be used with reactor waxes because of their dark color. The measurements were made in both the 0.05- and 0.23-m-ID glass columns with FT-300 wax, and only in the 0.05-m-ID glass column with the two reactor waxes. It was not possible to use this method with FT-300 wax for experiments with the 40-μm SMP distributor because of excessive foaming. Foaming was also observed at lower gas velocities ($\leq$0.05 m/s) during runs with FT-300 wax when the orifice-plate distributors were used, as shown in Figures 7 through 10, but the amount of foam produced was much smaller than in experiments with the SMP distributor. The broken lines in the holdup curves shown in these figures represent the foam breakage process.

Effect of Temperature. Figures 7a, 7b and 7c show the Sauter mean diameters, large bubble volume fraction, and average gas holdup, respectively, for experiments conducted with FT-300 wax in the 0.05-m-ID glass column. Results from experiments conducted at 200 and 265°C are compared in these figures. Two experiments were conducted at 265°C to check reproducibility of results. Rise velocities for the different bubble classes and the corresponding bubble sizes for one of the runs at 265°C (G2-2) are given in Table 3.

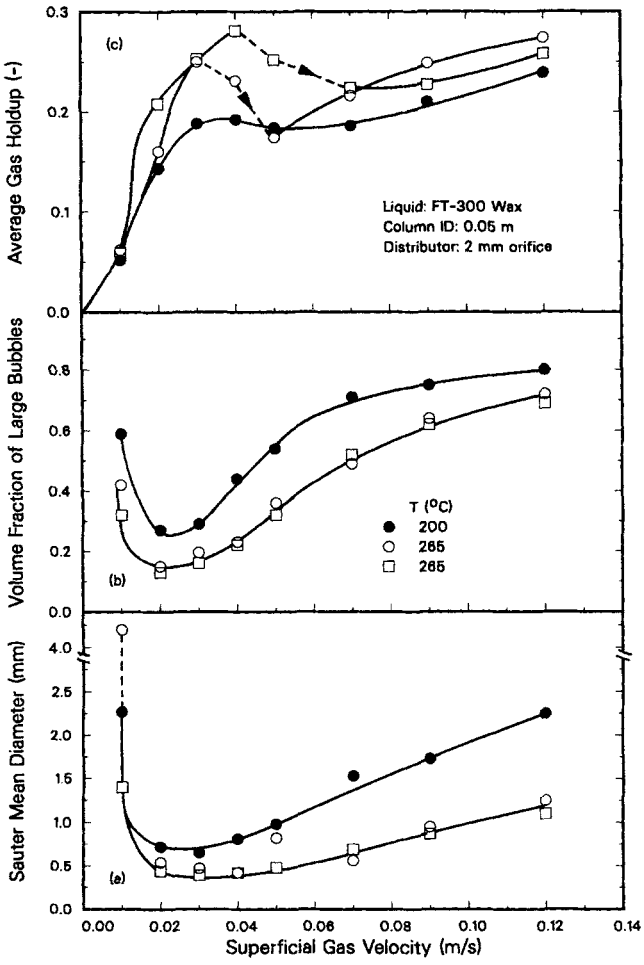

(a) Sauter mean bubble diameter
(b) Volume fraction of large bubbles
(c) Average gas holdup

Figure 7. Effect of temperature on hydrodynamic characteristics determined by DGD.

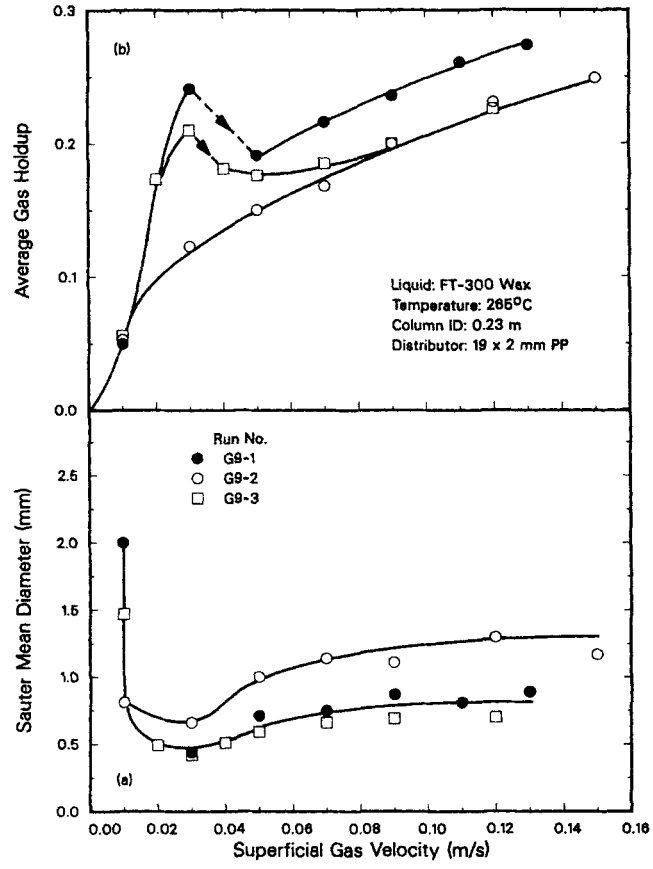

(a) Sauter mean bubble diameter
(b) Average gas holdup

Figure 8. Results from multiple runs in the large column using DGD.

Sauter mean diameter values for FT-300 wax at 265°C are consistently lower than those at 200°C, except at a gas velocity of 0.01 m/s. In runs at 265°C, foam was present at the top of the dispersion for the gas velocity range 0.02–0.05 m/s (Figure 7c). In this range d_s at 200°C is 50% higher than that at 265°C (0.75 mm vs. 0.5 mm). This difference increases with increasing gas velocity, and at a gas velocity of 0.12 m/s, d_s at 200°C is approximately twice as large as the value at 265°C (2 mm vs. 1 mm). The difference between d_s values at the two temperatures is due to the difference in the foaming tendency of the wax at the two temperatures. In the runs at 265°C, a significant amount of foam was present at the top of the dispersion at lower gas velocities ($\leq$0.05 m/s), whereas no foam was observed at 200°C (Figure 7c). For gas velocities greater than 0.05 m/s, the layer of foam collapsed in the runs at 265°C; however, fine bubbles continued to be present in the dispersion and d_s values remained lower than those obtained at 200°C. It is believed that the higher viscosity of FT-300 wax at 200°C (Table 2) prevented the formation of foam at this temperature. Results reported by

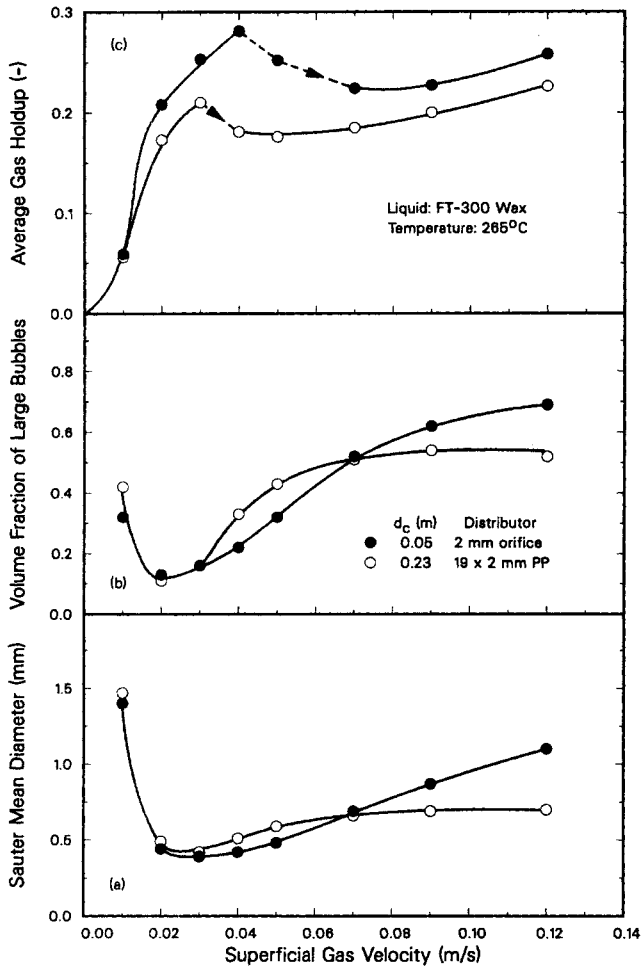

(a) Sauter mean bubble diameter
(b) Volume fraction of large bubbles
(c) Average gas holdup

Figure 9. Effect of column diameter on hydrodynamic characteristics determined by DGD.
○ Run G9-3; ● Run G2-2

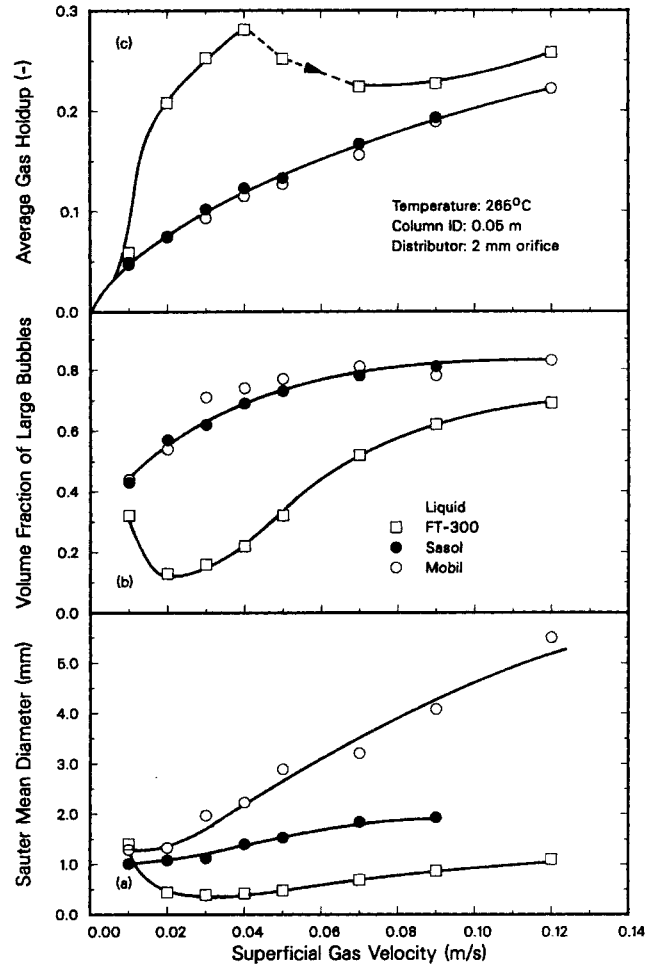

(a) Sauter mean bubble diameter
(b) Volume fraction of large bubbles
(c) Average gas holdup

Figure 10. Effect of wax type on hydrodynamic characteristics determined by DGD.
Run G2-2 used for FT-300 wax

Schügerl (1981) for experiments conducted with glycerine solutions show a similar effect of viscosity on bubble diameter.

Sauter mean bubble diameters at 200°C were greater than those at 265°C as a result of two effects:

1. The diameter of small bubbles at 200°C (~0.5 mm) is greater than that at 265°C (~0.3 mm).

2. The dispersion had a greater fraction of large bubbles at 200°C than that at 265°C (Figure 7b).

At both temperatures, the volume fraction of large bubbles reached a minimum at a gas velocity of 0.02 m/s and increased with increasing gas velocity, reaching as high as 80% at a gas velocity of 0.12 m/s at 200°C (mainly due to slugs). On comparing the trends in d_s and volume fraction of large bubbles (Figures 7a and 7b), it is clear that the gradual increase in d_s with increasing gas velocity is caused by a shift in the holdup structure from smaller bubbles at low gas velocities (0.02 m/s) to the larger class of bubbles at higher velocities (0.07–0.12 m/s).

Figure 7 also illustrates reproducibility of d_s values for the two runs conducted at 265°C. Results from the two runs are in very good agreement, except for discrepancies in d_s values at gas velocities of 0.01 and 0.05 m/s. The difference at the gas velocity of 0.05 m/s is because of differences in the amount of foam present. Foam had broken for Run G2-3, whereas it was still present in Run G2-2 (Figure 7c), causing d_s to be lower for the latter case. The discrepancy at the gas velocity of 0.01 m/s could be attributed to errors in the measurement process (small drop in height at low gas velocities).

The effect of temperature on d_s was also investigated with reactor waxes (Sasol's reactor wax and wax from Mobil's pilot-plant bubble column slurry reactor). Trends with these waxes were qualitatively similar to those obtained with FT-300 wax: i.e., larger d_s values were obtained at the lower temperature (Table 4).

Effect of Distributor Type. Dynamic gas disengagement measurements were made using the 2- and 4-mm-orifice plate distributors in the 0.05-m-ID glass column with FT-300 wax as the liquid medium. It was not possible to employ this technique for the run conducted using the 40-μm sintered metal plate distributor because of excessive foaming. All experiments were made at a temperature of 265°C. Results from these experiments (Table 3) showed that orifice diameter (2 mm or 4 mm) had no effect on either the holdup structure nor on d_s values.

Table 3. Dynamic Gas Disengagement Results for Selected Runs with FT-300 Wax

	Rise Velocities (m/s)			Bubble Sizes (mm)				
u_g(m/s)	u_{bS}	u_{bM}*	u_{bL}	d_{bS}	d_{bM}*	d_{bL}	d_s(mm)	d_s(mm)**
			Run G2-2, 265°C, 0.05 m ID column, 2 mm orifice					Run G2-1
0.01	0.10	0.15	0.23	0.8	1.8	9	1.4	2.3
0.02	0.03	—	0.30	0.4	—	17	0.4	0.7
0.03	0.02	—	0.31	0.3	—	18	0.4	0.7
0.04	0.02	—	0.30	0.3	—	17	0.4	0.8
0.05	0.02	—	0.38	0.3	—	29	0.5	1.0
0.07	0.02	—	0.36	0.3	—	25	0.7	1.5
0.09	0.02	—	0.47	0.3	—	44	0.9	1.7
0.12	0.02	—	0.51	0.3	—	48	1.1	2.3
			Run G2-4, 265°C, 0.05 m ID column, 4 mm orifice					
0.01	0.08	0.13	0.20	0.7	1.4	7	0.9	—
0.02	0.04	—	0.38	0.4	—	29	0.5	—
0.03	0.02	—	0.42	0.3	—	35	0.4	—
0.04	0.02	—	0.43	0.3	—	37	0.4	—
0.05	0.02	—	0.40	0.3	—	31	0.5	—
0.07	0.02	—	0.43	0.3	—	37	0.6	—
0.09	0.02	0.06	0.41	0.3	0.6	34	0.9	—
0.12	0.02	0.05	0.44	0.3	0.5	40	1.1	—
			Run G9-3, 265°C, 0.23 m ID column, 19 × 2 mm orifice					
0.01	0.10	0.12	0.21	0.9	1.1	7	1.5	—
0.02	0.03	0.06	0.48	0.4	0.5	46	0.5	—
0.03	0.02	—	0.46	0.3	—	42	0.4	—
0.04	0.02	—	0.51	0.3	—	52	0.5	—
0.05	0.02	—	0.51	0.3	—	53	0.6	—
0.07	0.02	—	0.54	0.3	—	58	0.7	—
0.09	0.02	—	0.56	0.3	—	63	0.7	—
0.12	0.02	0.06	0.54	0.3	0.5	58	0.7	—

*For cases where medium-size bubbles were detected
**Run conducted at 200°C

This is consistent with the findings of Miyahara et al. (1983), who showed that, for orifice plate distributors, even in the vicinity of the distributor bubble sizes are independent of the orifice diameter.

We were able to use the DGD technique for experiments conducted with reactor waxes at 265°C in the 0.05-m-ID column equipped with the 40-μm SMP distributor. These waxes are highly coalescing, relative to FT-300 wax, and do not have a tendency to foam (Bukur et al., 1987b). Sauter mean diameters with the SMP distributor were lower than d_s values obtained

Table 4. Dynamic Gas Disengagement Results for Selected Runs with Reactor Waxes

	Rise Velocities (m/s)			Bubble Sizes (mm)				
u_g(m/s)	u_{bS}	u_{bM}	u_{bL}	d_{bS}	d_{bM}	d_{bL}	d_s(mm)	d_s(mm)
			Sasol wax, 265°C, 0.05 m ID column, 2 mm orifice					200°C
0.01	0.04	0.13	0.34	0.4	1.1	23	1.0	3.3
0.02	0.04	0.07	0.33	0.4	0.6	21	1.1	1.7
0.03	0.04	0.07	0.36	0.4	0.6	24	1.1	2.9
0.04	0.04	0.07	0.38	0.4	0.6	29	1.4	3.0
0.05	0.04	0.07	0.41	0.4	0.6	34	1.5	3.8
0.07	0.03	0.06	0.40	0.3	0.5	32	1.8	3.8
0.09	0.03	0.07	0.51	0.3	0.6	53	1.9	4.5
0.12	—	—	—	—	—	—	—	4.6
			Mobil wax, 265°C, 0.05 m ID column, 2 mm orifice					200°C
0.01	0.03	0.16	0.29	0.4	3.1	16	1.3	1.9
0.02	0.03	0.10	0.38	0.4	0.9	31	1.3	2.7
0.03	0.03	0.08	0.38	0.4	0.7	31	2.0	3.1
0.04	0.03	0.09	0.40	0.4	0.7	32	2.2	3.7
0.05	0.03	0.12	0.42	0.4	1.4	36	2.9	5.2
0.07	0.03	0.10	0.49	0.4	1.1	47	3.2	5.0
0.09	0.03	0.17	0.52	0.4	3.9	52	4.1	7.5
0.12	0.04	0.17	0.49	0.4	3.9	47	5.5	8.2

with the 2-mm-orifice plate distributor. The difference was less than 20% at most velocities. This behavior is typical for coalescing media, where bubble sizes in fully established gas-liquid dispersions are independent of distributor type (e.g., Akita and Yoshida, 1974; Mersmann, 1978).

Effect of Column Diameter. Figures 8a and 8b show d_s and average gas holdup values for three runs conducted with FT-300 wax in the 0.23 m ID column at 265°C using the 19 × 2 mm perforated-plate distributor. Foam was produced in two of the three runs (G9-1 and G9-3), both of which were conducted in the increasing order of gas velocities, whereas foam was not produced in the experiment conducted in the decreasing order of gas velocities (Run G9-2). This hysteresis behavior in holdup often occurs in systems with foaming capacity (Bukur et al., 1987a, b). The differences in the holdup results are also reflected in the Sauter mean diameters for the three runs. Run G9-2, where foam was not observed, gave the highest d_s values as might be expected. Sauter mean bubble diameter values were similar for the two runs in which foam was present, even though the corresponding gas holdup values were different. These results show that d_s values for FT-300 wax in the churn turbulent flow regime ($u_g \geq 0.03$ m/s) are between 0.5–1.3 mm, depending on the amount of foam present.

The hysteresis behavior in gas holdups, like that depicted in Figure 8b, has been attributed to differences in the extent to which impurities are axially distributed in the liquid phase for increasing vs. decreasing order of gas velocities (Anderson and Quinn, 1970; Bukur et al., 1987b). Brief interruptions in gas flow, for recording the dynamic gas disengagement profile, do not affect the extent to which these impurities are dispersed in the column. This is because the only way, in which the impurities can be redistributed in the absence of gas flow, is through molecular diffusion, which is a slow process in liquids.

Figures 9a, 9b, and 9c illustrate the effect of column diameter on d_s, volume fraction of large bubbles, and average gas holdup, respectively, for experiments conducted with FT-300 wax at 265°C using the 2-mm-orifice plate in the 0.05 m ID column (Run G2-2) and the 19 × 2 mm perforated-plate distributor in the 0.23-m-ID glass column (Run G9-3). The two distributors are dynamically similar: i.e., for a given gas velocity the two give the same orifice Reynolds numbers (Re_o).

The effect of superficial gas velocity of d_s in the two columns is qualitatively similar, with values becoming constant at higher gas velocities ($u_g > 0.05$ m/s). The flow regimes in the two columns are different at gas velocities greater than about 0.03 m/s, i.e., slug flow in the small diameter column, and churn turbulent flow in the large diameter column. This difference manifests itself in the shapes of the curves shown in Figures 9a and 9b. The results shown in Table 3 indicate that the diameter of small bubbles was essentially the same in the two columns and did not vary much with gas velocity. However, the holdup structures in the two columns were different. The volume fraction of large bubbles (Figure 9b) in the 0.05-m-ID column increased steadily with gas velocity and reached 70% at 0.12 m/s, whereas in the large column it reached a constant value of around 50% for gas velocities above 0.05 m/s. Slugs in the small column are stabilized by the wall and continue to grow in length with an increase in gas velocity, with a concomitant increase in volume fraction of large bubbles. Large bubbles in the 0.23-m-ID column do not grow markedly with an increase in gas velocity (Table 3). This explains the differences in the trends observed for the variation of d_s with gas velocity in the two columns: i.e., in the large column (Figures 8a and 9a), d_s is essentially constant as gas velocity increases from 0.07 m/s to 0.12 m/s, while d_s in the small column shows an increase with gas velocity (Figure 9a).

Effect of Wax Type. Figures 10a, 10b and 10c show the effect of wax type on d_s, volume fraction of large bubbles, and average gas holdup, respectively. Holdup values for the two reactor waxes were very similar (Figure 10c), whereas higher holdups were obtained with FT-300 wax due to foam produced in the velocity range of 0.02–0.05 m/s. Rise velocities and bubble diameters for the reactor waxes are shown in Table 4.

Sauter mean diameters for the three waxes are significantly different as illustrated in Figure 10a. FT-300 wax shows a decrease in d_s as gas velocity is increased from 0.01 to 0.02 m/s and stays at about 0.5 mm when foam was present (0.02–0.05 m/s). It increases to about 1 mm with an increase in gas velocity. Sauter mean diameters for Sasol wax are around 1 mm at a gas velocity of 0.01 m/s and approach 2 mm for gas velocities greater than 0.05 m/s. With Mobil's reactor wax, d_s grows continuously from around 1 mm at a gas velocity of 0.01 m/s to 5.5 mm at 0.12 m/s. The volume fraction of large bubbles (Figure 10b) clearly distinguishes between the noncoalescing FT-300 wax and the highly coalescing reactor waxes. With reactor waxes, the concentration of large bubbles increases with gas velocity due to bubble coalescence. Whereas with FT-300 wax a large fraction of small bubbles remains entrained in the dispersion for gas velocities up to 0.05 m/s. However, at higher gas velocities, slugs begin to dominate and the holdup structure shifts to these large bubbles.

Despite similar holdup values and similar holdup structures, the two reactor waxes gave significantly different d_s values. Physical properties of the three systems are similar (Table 2), thus the differences in results may be attributed to differences in the concentration and/or nature of surface active impurities in these waxes (Bukur et al., 1987b). For experiments conducted with the three waxes at 200°C there were no differences in gas holdup values, but the Sauter mean bubble diameters followed the same trend as that observed at 265°C: i.e., d_s (FT-300 wax) < d_s (Sasol wax) < d_s (Mobil wax) (Tables 3 and 4). For each of the three waxes, d_s values at 200°C were greater than the corresponding values at 265°C due to the higher viscosity of the liquid medium.

Comments on the DGD technique

The Sauter mean bubble diameter is strongly influenced by the size of the smallest bubbles. Since the DGD technique relies on available rise velocity correlations to translate disengagement profiles to bubble-size distributions, the sensitivity of d_s to the type of correlation used was investigated. Two different correlations were used to estimate small bubble diameters and the resulting d_s values. The results from this analysis are shown in Table 5. The correlation proposed by Abou-el-Hassan (1983) resulted in d_s values that were consistently lower than those obtained when the correlation by Peebles and Garber (1953) was used. The sensitivity of d_s to the correlation used was less for FT-300 wax than it was for the reactor waxes. However, we believe that the variation in d_s with the type of correlation used is not significant considering the errors associated with such a technique. The overall effect of wax type on d_s is the same, irrespective of the correlation used.

Table 5. Sensitivity of d_s to Rise Velocity Correlation Used for Estimating Small Bubble Size*

	FT-300		Sasol		Mobil	
u_g (m/s)	d_s (mm)**	d_s (mm)†	d_s (mm)**	d_s (mm)†	d_s (mm)**	d_s (mm)†
0.01	1.4	1.9	1.0	1.3	1.3	1.6
0.02	0.4	0.6	1.1	1.6	1.3	1.6
0.03	0.4	0.4	1.1	1.6	2.0	2.4
0.04	0.4	0.4	1.4	2.1	2.2	2.8
0.05	0.5	0.5	1.5	2.2	2.9	3.7
0.07	0.7	0.8	1.8	2.7	3.2	4.0
0.09	0.9	0.9	1.9	2.7	4.1	4.5
0.12	1.1	1.2	—	—	5.5	6.3

*Data taken from runs conducted at 265°C, in the 0.05-m-ID column with the 2-mm-orifice plate

**Using Abou-el-Hassan (1983) correlation for small and medium bubbles

†Using Pebbles and Garber (1953) correlation for small and medium bubbles

Visual observations of the dispersion at gas velocities greater than 0.05 m/s indicate that large bubbles (slugs) are present in the dispersion in the 0.05-m-ID column. However, the large bubble rise velocities shown in Tables 3 and 4, for this range of gas velocities, do not conform with these observations. The terminal rise velocity for a slug in this column should be 0.25 m/s (Patel et al., 1989); however, u_{bL} values shown in Tables 3 and 4 are significantly higher than this value. The implications are that large bubbles observed in the molten waxes are not impeded by the wall as would be expected, instead they continue to rise as if the wall drag was absent. Buchholz et al. (1978) also reported a similar enhancement of large bubble rise velocities in the presence of small bubbles with carboxymethyl cellulose (CMC) solutions in a 0.14-m-ID column. When the same technique was used with the tap water system (Patel et al., 1989), large bubble rise velocity stabilized at 0.28 m/s once slugs appeared in the dispersion, as expected. The primary difference between the different systems is the presence or absence of fine bubbles. It appears that small bubbles have an effect on rise velocities of large bubbles, and further studies are required to clarify these observations.

Comparison of bubble-size measurement techniques

The dynamic gas disengagement technique gives an average value of the Sauter mean diameter for the entire column, whereas the photographic technique provides point estimates for d_s.

In Figure 11 d_s values obtained for FT-300 wax in the large columns (0.23-m-ID glass or 0.24-m-ID stainless steel) using the DGD technique are compared with those obtained from photographs taken near the wall and near the center of the column. Results from the DGD method are represented by the shaded region in Figure 11 to indicate the variability in d_s values (see Figure 8). These results show that Sauter mean diameters obtained using photography at the column center lie in the range of values obtained using DGD for gas velocities greater than 0.04 m/s. However, d_s values obtained from photographs at the column wall, for the same range of gas velocities, fall below the range of values obtained from DGD. This is as expected, since DGD gives an average Sauter mean diameter for the entire dispersion (i.e., it accounts for bubbles near the center and those

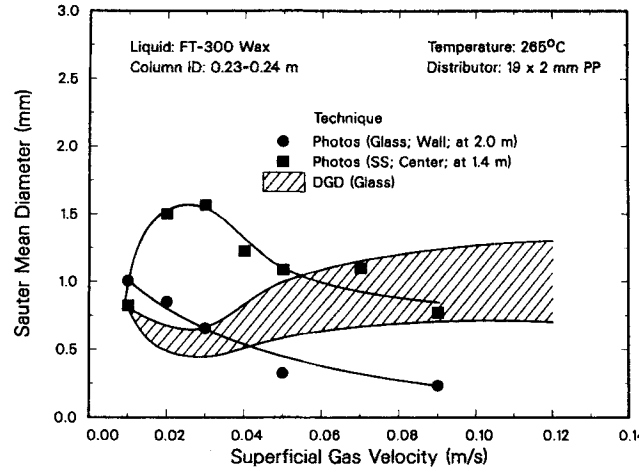

Figure 11. Comparison of Sauter mean bubble diameters from the photographic and the dynamic gas disengagement techniques.

near the column wall). Furthermore, the larger bubbles (greater than 15 to 20 mm in diameter), present in the dispersion at higher gas velocities (≥0.05 m/s), were taken into consideration in the DGD results, whereas they were not included in the photographic data. This is because only an area of 15 × 20 mm was photographed. The d_s values from DGD at lower gas velocities (≤0.04 m/s), where foam was present, are lower than those obtained from photographs taken near the center of the column. Results from DGD and photography suggest that the Sauter mean diameter for FT-300 wax at 265°C is in the range of 0.6–1.5 mm. Furthermore, at 265°C, d_s value from DGD in the presence of foam is consistently around 0.5 mm, which is the same as that obtained when photographs of pure foam were analyzed.

Figure 12 compares the size of small bubbles obtained from DGD with those obtained from photographic measurements near the column wall in the 0.23-m-ID column. The photographs were taken just after the large bubbles had left the dispersion following the shutting off of gas flow to the column at a given gas velocity. Visual observations indicate that the disper-

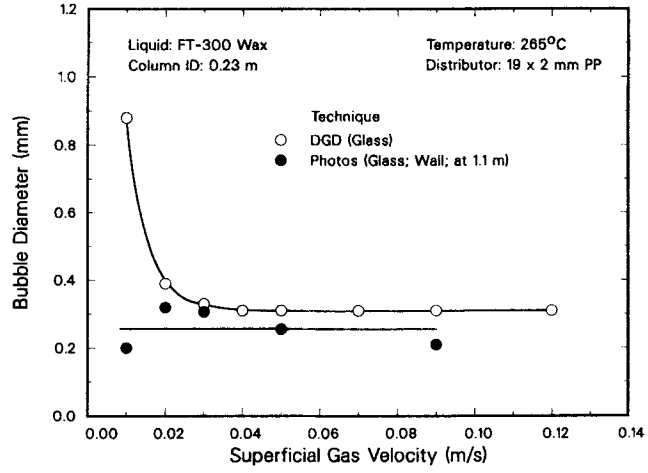

Figure 12. Comparison of small bubble diameters estimated from the photographic and the dynamic gas disengagement techniques.

sion consists of only the small bubbles. Arithmetic average bubble diameters are used for values taken from photographic measurements. The excellent agreement between small bubble diameter estimates from DGD and photography (for gas velocities greater than 0.01 m/s) indicates the viability of the DGD technique as an alternative to the photographic method.

Summary and Conclusions

Our results show that systems having similar physical properties can have vastly different holdups and/or bubble-size distributions. This has been demonstrated using molten wax—nitrogen systems, which are of interest in slurry-phase Fischer-Tropsch synthesis. At low gas velocities ($\leq$0.05 m/s), FT-300 wax has a tendency to foam, and d_s values for this medium are considerably lower than those for reactor waxes. However, at higher gas velocities (>0.05 m/s), holdups for the different waxes are similar, but d_s values are significantly different. FT-300 wax has the highest specific gas-liquid area, while Mobil's reactor wax has the lowest area available for mass transfer.

Sauter mean diameters obtained with FT-300 wax are in good agreement with literature values. Also, there is very good agreement between results obtained by photography and those obtained by dynamic gas disengagement for this wax. In the presence of foam, both techniques gave d_s values of about 0.5 mm. Sauter mean diameters at higher gas velocities (>0.05 m/s) are in the range of 0.6–1.3 mm for FT-300 wax at 265°C. Our results also indicate that, for $u_g \geq 0.03$ m/s, radial profiles for d_s are no longer uniform, implying that the photographic technique at these velocities may give erroneous results if used only at the wall. The holdup structures in the 0.05- and 0.23-m-ID columns reflect the differences in flow regimes for the two columns. The volume fraction of large bubbles in the small column increases as the gas velocity increases (growing number and size of slugs), whereas it remains fairly constant in the large column (churn-turbulent flow regime). Sauter mean diameters for Sasol's Arge reactor wax at 265°C, determined by the DGD method, approach 2 mm at gas velocities greater than 0.05 m/s, and those for Mobil's reactor wax increase with increasing gas velocity and reach a value of 5.5 mm at a gas velocity of 0.12 m/s. These values are comparable to those obtained in the earlier studies with similar waxes (d_s = 2–4 mm), where different experimental techniques were employed (Calderbank et al., 1963; O'Dowd et al., 1986).

Dynamic gas disengagement appears to be a viable technique for estimating bubble-size distributions in bubble columns.

Acknowledgment

The financial support of the U. S. Department of Energy (Contract DE-AC22-84PC70027) is gratefully acknowledged. Sasol wax was kindly supplied by John McArdle of UOP Inc. with permission from Dr. Mark Dry of SASOL, and Mobil's reactor wax was obtained from DOE Pittsburgh Energy Technology Center through courtesy of Mobil Research and Development Co. The authors would like to thank John Swank and Matheo Raphael for their help with the experiments, and Dr. Malcolm Brown of The University of Texas at Austin, for allowing us to use the image analysis system.

Notation

a = specific gas-liquid interfacial area, m^{-1}
b_i = intercept associated with the ith line
d_b = bubble diameter, mm
d_{bi} = diameter of a bubble in the ith class, mm
d_c = column diameter, m
d_o = orifice diameter, mm
d_s = Sauter mean bubble diameter, mm
d_s^* = Sauter mean bubble diameter at the orifice, mm
F = flow number
g = acceleration due to gravity, m/s^2
H = dispersion height, m
H_s = static or ungassed liquid height, m
n_i = number of bubbles in class i
Re = Reynolds number, $d_{bS}u_{b\infty}\rho_\ell/\mu_\ell$
Re_o = orifice Reynolds number, $d_o u_o \rho_\ell/\mu_\ell$
s_i = slope associated with the ith line, s^{-1}
t = time, s
u_b = bubble rise velocity, m/s
u_{bi} = rise velocity for bubbles in the ith class, m/s
$u_{b\infty}$ = terminal rise velocity of a single bubble or slug, m/s
u_g = superficial gas velocity, m/s
u_o = gas velocity through the orifice, m/s
V = velocity number

Greek letters

ϵ_g, ϵ_{go} = average gas hold-up
ϵ_{goi} = hold-up associated with bubbles in the ith class
μ = viscosity, mPa.s, or mean
ρ = density, kg/m^3
σ = surface tension, N/m, or standard deviation

Subscripts

g = gas
ℓ = liquid
L = large bubbles
M = medium bubbles
o = at time $t = 0$, related to the orifice
S = small bubbles

Literature Cited

Abou-el-Hassan, M. E., "A Generalized Bubble Rise Velocity Correlation," *Chem. Eng. Commun.*, **22**, 243 (1983).

Akita, K., and F. Yoshida, "Bubble Size, Interfacial Area, and Liquid-Phase Mass Transfer in Bubble Columns," *Ind. Eng. Chem. Process Des. Dev.*, **13**, 84 (1974).

Anderson, J. L., and J. A. Quinn, "Bubble Columns: Flow Transitions in the Presence of Trace Contaminants," *Chem. Eng. Sci.*, **25**, 373 (1970).

Bhavaraju, S. M., T. W. F. Russell, and H. W. Blanch, "The Design of Gas Sparged Devices for Viscous Liquid Systems," *AIChE J.*, **24**, 454 (1978).

Buchholz, H., R. Buchholz, J. Lücke, and K. Schügerl, "Bubble Swarm Behaviour and Gas Absorption in Non-Newtonian Fluids in Sparged Columns," *Chem. Eng. Sci.*, **33**, 1061 (1978).

Buchholz, R., and K. Schügerl, "Methods for Measuring the Bubble Size in Bubble Column Bioreactors: II," *Europ. J. Appl. Microbiol. Biotechnol.*, **6**, 315 (1979).

Bukur, D. B., D. Petrovič, and J. G. Daly, "Hydrodynamics of Fischer-Tropsch Synthesis in Slurry Bubble Column Reactors," *Proc. DOE Indirect Liquefaction Contractors' Mtg.*, Houston, 479 (Dec. 2–5, 1985).

———, "Flow Regime Transitions in a Bubble Column with a Paraffin Wax as the Liquid Medium," *Ind. Eng. Chem. Res.*, **26**, 1087 (1987a).

Bukur, D. B., S. A. Patel, and R. Matheo, "Hydrodynamic Studies in Fischer-Tropsch Derived Waxes in a Bubble Column," *Chem. Eng. Commun.*, **60**, 63 (1987b).

Bukur, D. B., and J. G. Daly, "Gas Hold-Up in Bubble Columns for Fischer-Tropsch Synthesis," *Chem. Eng. Sci.*, **42**, 2967 (1987).

Bukur, D. B., and S. A. Patel, "Hydrodynamic Studies with Foaming and Non-Newtonian Solutions in Bubble Columns," *Can. J. Chem. Eng.*, in press (1989).

Calderbank, P. H., F. Evans, R. Farley, G. Jepson, and A. Poll, "Rate Processes in the Catalyst-Slurry Fischer-Tropsch Reaction," *Catalysis in Practice—Instn. Chem. Engrs.*, 66 (1963).

Clift, R., J. R. Grace, and M. E. Weber, *Bubble Drops and Particles,* Academic Press, New York, 171 (1978).
Deckwer, W.-D., Y. Louisi, A. Zaidi, and M. Ralek, "Hydrodynamic Properties of the Fischer-Tropsch Slurry Process," *Ind. Eng. Chem. Process Des. Dev.*, **19,** 699 (1980).
Fan, L. S., *Gas-Liquid-Solid Fluidization Engineering,* Butterworth Publishers, Boston, 298 (1989).
Heijnen, J. J., and R. K. van't Riet, "Mass Transfer, Mixing and Heat Transfer Phenomena in Low Viscosity Bubble Column Reactors," *Chem. Eng. J.*, **28,** B21 (1984).
Kölbel, H., and M. Ralek, "The Fischer-Tropsch Synthesis in the Liquid Phase," *Cat. Rev. Sci. Eng.*, **21,** 225 (1980).
Kuo, J. C. W., "Two-Stage Process for Conversion of Synthesis Gas to High Quality Transportation Fuels," Mobil Research and Development's Final Report to the Dept. of Energy for Contract DE-AC22–83PC60019 (1985).
Mersmann, A., "Design and Scale-up of Bubble and Spray Columns," *Ger. Chem. Eng.*, **1,** 1 (1978).
Miyahara, T., N. Haga, and T. Takahashi, "Bubble Formation from an Orifice at High Gas Flow Rates," *Int. Chem. Eng.*, **23,** 524 (1983).
O'Dowd, W., D. N. Smith, and J. A. Ruether, "Slurry F-T Hydrodynamics and Scale-Up," *Proc. DOE Indirect Liquefaction Contractors' Mtg.*, Monroeville, PA, 147 (Dec. 2–4, 1986).
Patel, S. A., J. G. Daly, and D. B. Bukur, "Holdup and Interfacial Area Measurements Using Dynamic Gas Disengagement," *AIChE J.*, **35,** 931 (1989).
Peebles, F. N., and H. J. Garber, "Studies on the Motion of Gas Bubbles in Liquids," *Chem. Eng. Prog.*, **49,** 88 (1953).
Quicker, G., and W.-D. Deckwer, "A Further Note on Mass Transfer Limitations in the Fischer-Tropsch Slurry Process," *Chem. Eng. Sci.*, **36,** 1577 (1981).
Sanders, E., S. Ledakowicz, and W.-D. Deckwer, "Fischer-Tropsch Synthesis in Bubble Column Slurry Reactors on Fe/K-Catalyst," *Can. J. Chem. Eng.*, **64,** 133 (1986).
Satterfield, C. N., and G. A. Huff, "Effects of Mass Transfer on Fischer-Tropsch Synthesis in Slurry Reactors," *Chem. Eng. Sci.*, **35,** 195 (1980).
Saxena, S. C., D. Patel, D. N. Smith, and J. A. Ruether, "An Assessment of Experimental Techniques for the Measurement of Bubble Size in a Bubble Slurry Reactor as Applied to Indirect Coal Liquefaction," *Chem. Eng. Comm.*, **63,** 87 (1988).
Schügerl, K., "Oxygen Transfer into Highly Viscous Media," *Adv. Biochem. Eng.*, **7,** 1 (1981).
Shah, Y. T., B. G. Kelkar, S. P. Godbole, and W.-D. Deckwer, "Design Parameters Estimations for Bubble Column Reactors," *AIChE J.*, **28,** 353 (1982).
Smith, D. N., J. A. Ruether, and G. J. Stiegel, "Slurry Bubble Column Dynamics," *Proc. DOE Indirect Liquefaction Contractors' Mtg.*, Pittsburgh, 9-1 (Oct. 12–13, 1983).
Smith, D. N., W. Fuchs, R. J. Lynn, D. H. Smith, and M. Hess, "Bubble Behavior in a Slurry Bubble Column Reactor Model," *Chemical and Catalytic Reactor Modeling, ACS Symp. Ser.*, M. P. Dudukovic and P. L. Mills, eds., **237,** 125 (1984).
Sriram, K., and R. Mann, "Dynamic Gas Disengagement: a New Technique for Assessing the Behavior of Bubble Columns," *Chem. Eng. Sci.*, **32,** 571 (1977).
Ueyama, K., S. Morooka, K. Koide, H. Kaji, and T. Miyauchi, "Behavior of Gas Bubbles in Bubble Columns," *Ind. Eng. Chem. Proc. Des. Dev.*, **19,** 592 (1980).
Zaidi, A., Y. Louisi, M. Ralek, and W.-D. Deckwer, "Mass Transfer in the Liquid Phase Fischer-Tropsch Synthesis," *Ger. Chem. Eng.*, **2,** 94 (1979).

Manuscript received July 5, 1989, and revision received Oct. 24, 1989.